IMMUNOLOGY

Dipeptidase-1 governs renal inflammation during ischemia reperfusion injury

Arthur Lau[1], Jennifer J. Rahn[1], Mona Chappellaz[1], Hyunjae Chung[1], Hallgrimur Benediktsson[2], Dominique Bihan[3], Anne von Mässenhausen[4], Andreas Linkermann[4], Craig N. Jenne[5], Stephen M. Robbins[6]†, Donna L. Senger[6]†, Ian A. Lewis[3], Justin Chun[1], Daniel A. Muruve[1]*

The mechanisms that drive leukocyte recruitment to the kidney are incompletely understood. Dipeptidase-1 (DPEP1) is a major neutrophil adhesion receptor highly expressed on proximal tubular cells and peritubular capillaries of the kidney. Renal ischemia reperfusion injury (IRI) induces robust neutrophil and monocyte recruitment and causes acute kidney injury (AKI). Renal inflammation and the AKI phenotype were attenuated in *Dpep1*$^{-/-}$ mice or mice pretreated with DPEP1 antagonists, including the LSALT peptide, a nonenzymatic DPEP1 inhibitor. DPEP1 deficiency or inhibition primarily blocked neutrophil adhesion to peritubular capillaries and reduced inflammatory monocyte recruitment to the kidney after IRI. CD44 but not ICAM-1 blockade also decreased neutrophil recruitment to the kidney during IRI and was additive to DPEP1 effects. DPEP1, CD44, and ICAM-1 all contributed to the recruitment of monocyte/macrophages to the kidney following IRI. These results identify DPEP1 as a major leukocyte adhesion receptor in the kidney and potential therapeutic target for AKI.

INTRODUCTION

Acute kidney injury (AKI) is a significant clinical problem for which no specific therapies, aside from supportive care, currently exist. Patients who experience AKI in several contexts are at higher risk of cardiovascular events, chronic or end-stage kidney disease, and death (*1*, *2*). Renal ischemia reperfusion injury (IRI) is a major cause of AKI. A reduction in renal blood flow followed by reperfusion during patient recovery occurs in numerous clinical contexts including cardiac surgery and kidney transplantation (*3*–*5*).

Renal IRI triggers inflammation and leukocyte infiltration to the tubulointerstitial compartment as well as tubular cell death via several mechanisms that include necroptosis and ferroptosis (*6*, *7*). The inflammatory response plays a significant role in the pathophysiology of AKI, and several experimental studies have demonstrated improved clinical AKI phenotypes when inflammation is blocked (*8*, *9*). Consistent with these studies, biomarkers of inflammation are commonly observed in patients with AKI (*10*, *11*). Despite these findings, mechanisms that drive inflammation and leukocyte recruitment to the kidney during injury are not well understood.

The recruitment of neutrophils and other leukocytes from the blood into injured or infected tissues is a multistep process that differs between tissues. The classical recruitment process for vascular beds within the muscle, mesentery, and skin requires the initial tethering and rolling of the neutrophil that is mediated by selectins (e.g., E- and P-selectin) on endothelial cells and their counter-receptors (e.g., P-selectin glycoprotein ligand-1) on neutrophils, followed by firm adhesion to the integrin family of receptors (*12*). Neutrophil recruitment to the liver and lungs, however, does not follow this classical cascade but appears to require distinct mechanism(s) (*13*, *14*). In the kidney, studies in models of renal IRI have demonstrated a role for P-selectin, E-selectin, intercellular adhesion molecule–1 (ICAM-1), and CD44 expressed in peritubular capillaries in leukocyte recruitment (*15*–*18*). Blocking ICAM-1, CD44, or corresponding leukocyte integrin ligands using pharmacologic or genetic approaches prevents leukocyte adhesion in the kidney and improves the IRI phenotype. However, targeting single pathways during IRI only partially prevents leukocyte recruitment, suggesting that alternate pathways exist (*15*, *16*, *18*, *19*).

Dipeptidase-1 (DPEP1) is a glycosylphosphatidylinositol-anchored, disulfide-linked, glycosylated homodimer highly expressed in the brush border of proximal tubular epithelial cells (*20*–*22*). DPEP1 is classically known to hydrolyze dipeptides and is involved in glutathione and leukotriene metabolism (*23*). DPEP1 also metabolizes the beta-lactam ring of thienamycin antibiotics and is the target of the enzymatic inhibitor cilastatin, a drug developed specifically to increase the half-life of the antibiotic imipenem (*23*, *24*). Studies from our group and others (*25*–*27*) have identified a role for DPEP1 in toxin-induced AKI triggered by agents such as radiographic contrast and cisplatin.

Recently, our group uncovered a previously unidentified role for DPEP1 in leukocyte adhesion to endothelium in the lungs and liver during sepsis (*14*). The mechanism is independent of DPEP1's enzymatic activity and likely involves a direct interaction with an as yet uncharacterized ligand on leukocytes. Given the abundant expression of DPEP1 in the kidney, we postulated that DPEP1 could also play a role in renal inflammation in the context of nonmicrobial and non–drug-induced kidney injury. In this study, we show that DPEP1 regulates the adhesion of neutrophils and monocytes to the peritubular capillaries during renal IRI and contributes to the severity of AKI.

[1]Department of Medicine, Snyder Institute for Chronic Diseases, Cumming School of Medicine, University of Calgary, Calgary, AB, Canada. [2]Department of Pathology and Laboratory Medicine, Snyder Institute for Chronic Diseases, Cumming School of Medicine, University of Calgary, Calgary, AB, Canada. [3]Department of Biological Sciences, University of Calgary, Calgary, Canada. [4]Division of Nephrology, Department of Internal Medicine 3, University Hospital Carl Gustav Carus and Biotechnology Center, Technische Universität Dresden, Dresden 01307, Germany. [5]Department of Microbiology, Immunology and Infectious Diseases, Snyder Institute for Chronic Diseases, Cumming School of Medicine, University of Calgary, Calgary, AB, Canada. [6]Department of Oncology, Arnie Charbonneau Cancer Institute, Cumming School of Medicine, University of Calgary, Calgary, AB, Canada.
*Corresponding author. Email: dmuruve@ucalgary.ca
†Present address: Lady Davis Institute for Medical Research at the Jewish General Hospital, Montreal, PQ, Canada.

RESULTS

DPEP1 expression in the kidney

DPEP1 was first identified in the brush border of the rat proximal tubule and characterized as an enzyme that metabolized the dipeptide cysteinylglycine, leukotriene D4, and the beta-lactam ring of antibiotics such as imipenem (*21*–*23*). Consistent with these findings, immunohistochemistry confirmed DPEP1 expression primarily in the proximal tubule of the normal human kidney (Fig. 1A). Recently, our group identified a previously unknown role for endothelium-expressed DPEP1 in neutrophil recruitment to the lungs and liver (*14*). Endothelial cell activation was required to modulate DPEP1's leukocyte adhesion capability. Given the minimal expression of DPEP1 on vascular endothelium in normal kidney, we next assessed DPEP1 expression in allograft biopsies of kidney transplant patients who experienced IRI, without rejection, early after transplant. Increased DPEP1 expression could be identified in the peritubular capillaries of injured kidneys (Fig. 1A). In mice, DPEP1 protein expression increased in total kidney homogenates within 8 hours of IRI or systemic lipopolysaccharide (LPS) administration (Fig. 1, B and C). IRI and LPS also induced a slight increase in DPEP1 molecular mass consistent with additional posttranslational modification that may underlie its leukocyte adhesion properties (*14*). To localize DPEP1 expression in mouse kidneys, tissues were assessed by conventional immunohistochemistry and probed with fluorescent-labeled LSALT, a DPEP1-binding peptide and nonenzymatic DPEP1 inhibitor (*14*). In normal mouse kidney, DPEP1 expression was seen primarily not only in the brush border of proximal tubular cells but also in the peritubular capillary network, as observed in the human kidney (Fig. 1, D and E). Following IRI or systemic LPS administration, DPEP1 expression and LSALT peptide binding increased substantially in both compartments, especially in the peritubular capillaries (Fig. 1, D and E). DPEP1 expression and induction on kidney endothelium and epithelium, but not infiltrating leukocytes, following renal IRI and LPS administration were verified by flow cytometry (Fig. 1F). These data confirm DPEP1 expression in the kidney epithelium and endothelium at baseline and up-regulation following injury.

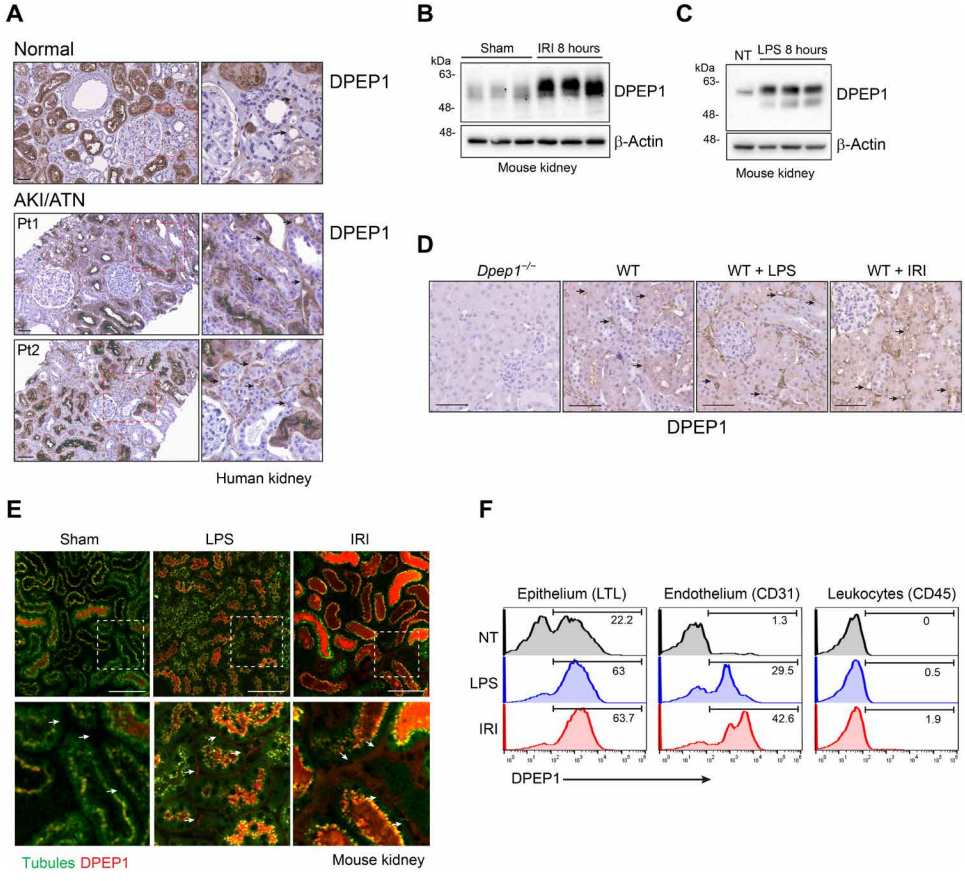

Fig. 1. DPEP1 expression in the kidney. (**A**) DPEP1 immunohistochemistry in normal human kidney and allograft biopsies with clinical ATN/acute tubular necrosis (ATN). Arrows denote peritubular capillaries. Pt1 and Pt2 denote biopsies from 2 individual patients. Scale bars, 50 μm. Right panels are magnification of hatched boxes. (**B** and **C**) Immunoblot probing for DPEP1 in kidney lysates from mice treated with renal IRI and lipopolysaccharide (LPS) at 8 hours. Sham and untreated (NT) mice are controls. (**D**) DPEP1 **i**mmunohistochemistry in wild-type (WT) mouse kidneys following IRI or LPS treatment at 8 hours. Kidney from untreated *Dpep1*$^{-/-}$ mouse is used as a control. Arrows denote peritubular capillaries. Scale bars, 50 μm. (**E**) Kidney IVM in mice following sham operation, LPS administration, and IRI (8 hours). Tubules are visualized using autofluorescence and DPEP1 expression by fluorescent-labeled LSALT peptide. Arrows denote peritubular capillaries. Labels: tubules (green) and DPEP1 (red). Scale bars, 100 μm. Bottom panels are magnification of hatched boxes. (**F**) Representative flow cytometry for DPEP1 expression in cells isolated from the kidneys of untreated (NT), LPS-, or IRI-treated mice (8 hours). Cells sorted using LTL (proximal tubular epithelial cells), CD31 (endothelial cells), and CD45 (leukocytes).

DPEP1 mediates leukocyte adhesion in the kidney

DPEP1 is a neutrophil adhesion receptor in the lungs and liver during endotoxemia and sepsis (*14*). To determine the role of DPEP1 in nonmicrobial kidney inflammation, leukocyte recruitment was assessed using intravital microscopy (IVM) in *Dpep1*$^{-/-}$ mice undergoing IRI. A robust influx of adherent CD11b^{+} leukocytes was observed in the peritubular capillaries of wild-type kidneys within 2 hours of IRI, a response that was significantly less in the kidneys of *Dpep1*$^{-/-}$ mice (Fig. 2, A and B). Next, experiments were performed to assess renal inflammation following pharmacologic inhibition of DPEP1. LSALT is a DPEP1 targeting peptide that blocks DPEP1-mediated leukocyte adhesion but not DPEP1 enzymatic activity (*14*). Using IVM in *LysM*$^{gfp/gfp}$ reporter mice that express green fluorescent protein (GFP) in myelomonocytic cells (neutrophils and circulating monocyte/macrophages) (*28*), LSALT peptide, but not scrambled peptide, inhibited the recruitment of GFP^{+} leukocytes to the kidney in a dose-dependent manner at 2 hours following IRI (Fig. 2, C to F). Since IVM can only visualize the superficial renal cortex, flow cytometry was used to characterize total kidney leukocyte populations affected by DPEP1 deficiency or pharmacologic inhibition (Fig. 3 and fig. S1). At 24 hours after IRI, a significant reduction of both neutrophils and inflammatory monocytes was seen. At 48 hours, DPEP1 inhibition or deficiency affected mainly neutrophil recruitment and less so inflammatory monocytes, perhaps because of the changing phenotype of macrophages that occurs in this model at this time point (*8*). DPEP1 inhibition using LSALT peptide had minimal impact on other leukocyte populations such as lymphocytes and natural killer (NK) cells (fig. S2). Last, similar experiments were performed using the small-molecule DPEP1 enzymatic inhibitor, cilastatin (*24*), and an alternate DPEP1-binding peptide, GFE-1 (*29*). As observed with LSALT peptide, both cilastatin and GFE-1 inhibited early leukocyte recruitment to the kidney following IRI in *LysM*$^{gfp/gfp}$ mice as determined by IVM (Fig. 4, A and B). Cilastatin induced similar changes in total leukocyte populations at 48 hours following IRI as seen in LSALT peptide–treated or *Dpep1*$^{-/-}$ mice. Flow cytometry of total kidney leukocyte populations revealed a greater reduction in neutrophils rather than inflammatory monocytes following IRI and cilastatin treatment (Fig. 4, C and D). These data show that DPEP1 is involved in leukocyte recruitment to the kidney during IRI, an effect that can be targeted pharmacologically.

DPEP1 antagonists abrogate ischemia reperfusion–induced AKI

Several studies have demonstrated the effectiveness of inhibiting general leukocyte recruitment to improve the renal phenotype of experimental AKI (*16*, *18*, *19*). To assess whether inhibiting DPEP1-mediated inflammation would affect the ischemia reperfusion–induced AKI, phenotypic studies of renal injury were performed. Consistent with the effects observed on leukocyte populations, *Dpep1*$^{-/-}$ mice demonstrated less kidney injury molecule-1 (KIM-1) expression, a marker of tubular injury, and improved kidney function at 48 hours after IRI in a single kidney nephrectomy model (Fig. 5, A and B). Similarly, pretreatment of mice with cilastatin or the LSALT peptide also attenuated the up-regulation of KIM-1 and improved kidney function, as measured by serum creatinine (Fig. 5, C and D). In all cases, the improved AKI phenotype was associated with a reduction in tubulointerstitial neutrophils, as seen by immunofluorescence microscopy (Fig. 5, A and C). Thus, inhibiting DPEP1-mediated leukocyte recruitment using pharmacologic and genetic approaches reduces the severity of experimental AKI.

DPEP1 is a major leukocyte adhesion molecule in the kidney

Leukocyte recruitment to the kidney is incompletely understood. CD44 and ICAM-1 have previously been identified as key leukocyte

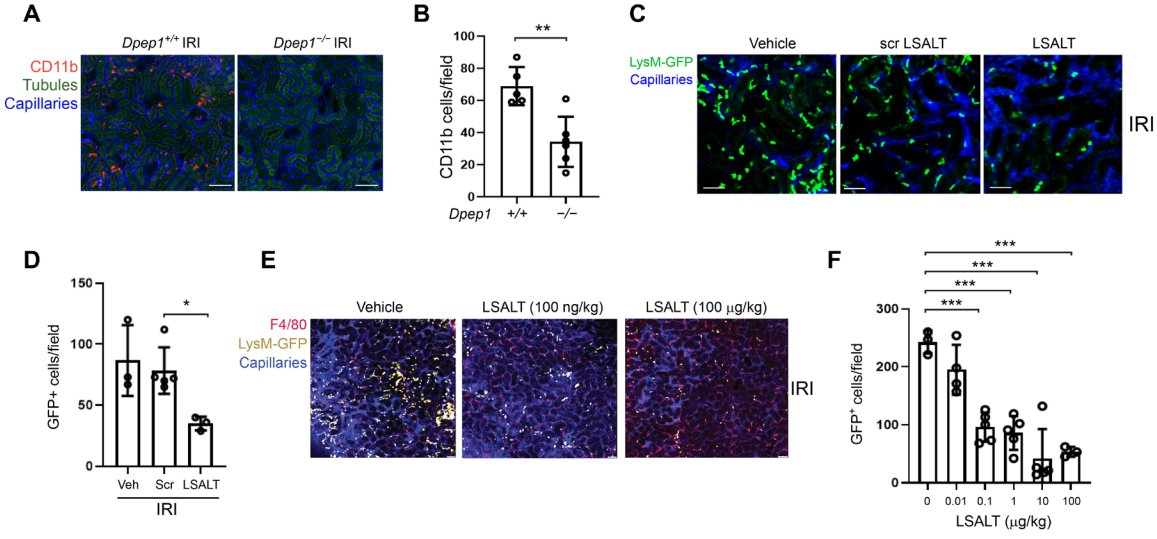

Fig. 2. DPEP1 and leukocyte recruitment during kidney IRI. (**A**) Kidney IVM in *Dpep1*$^{+/+}$ and *Dpep1*$^{-/-}$ mice at 2 hours following renal IRI. Labels: leukocytes (CD11b, red), tubules (autofluorescence, green), and capillaries (QTracker, blue). Scale bars, 100 μm. (**B**) Quantification of stationary CD11b^{+} cells/field in the kidney (*Dpep1*$^{+/+}$ versus *Dpep*$^{1-/-}$, $^{**}P = 0.003$, $n = 5$ to 6 per group, Student's *t* test). (**C**) Kidney IVM in *LysM*$^{gfp/gfp}$ mice 2 hours following IRI. Mice were pretreated with vehicle (phosphate-buffered saline), scrambled (Scr) LSALT peptide, or LSALT peptide. Labels: leukocytes (LysM-GFP, bright green) and capillaries (QTracker, blue). Scale bars, 50 μm. (**D**) Quantification of stationary GFP^{+} leukocytes/field in the kidneys of mice 2 hours after IRI treatment with vehicle, LSALT peptide, or scrambled LSALT peptide (LSALT peptide versus scrambled peptide, $^{*}P = 0.03$, $n = 3$ to 5). (**E**) Kidney IVM and (**F**) quantification of stationary GFP^{+} leukocytes in *LysM*$^{gfp/gfp}$ mice 2 hours after IRI treatment with increasing doses of LSALT peptide. Labels: macrophages (F4/80, red), leukocytes (LysM-GFP, yellow), tubules (autofluorescence, dark green), and capillaries (QTracker, blue) [LSALT peptide 0 μg/kg versus 0.1 μg/kg, $^{***}P = 0.0002$; 1 μg/kg, $^{***}P = 0.0001$; 10 μg/kg, $^{***}P = 0.0003$; 100 μg/kg, $^{***}P = 0.0001$; $n = 3$ to 5 per group, analysis of variance (ANOVA) with Dunnett's post hoc test].

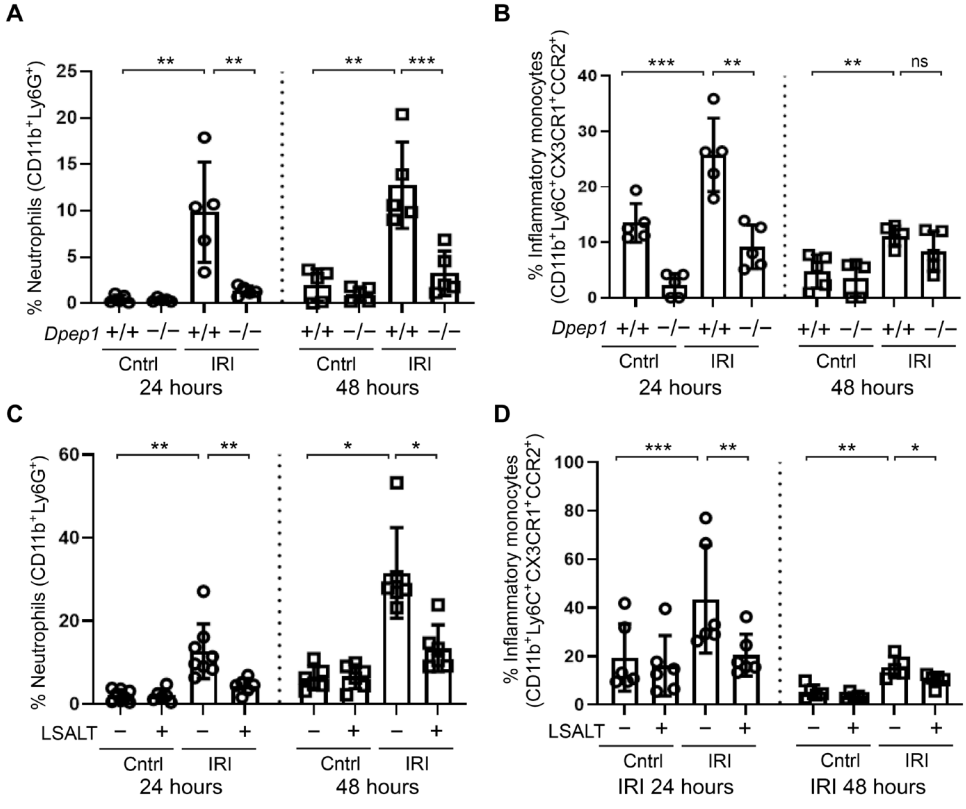

Fig. 3. DPEP1-mediated neutrophil and inflammatory monocyte recruitment to the injured kidney. Flow cytometry of neutrophil (**A**) and inflammatory monocyte (**B**) recruitment to the kidneys of *Dpep1*$^{+/+}$ and *Dpep1*$^{-/-}$ at 24 hours (circles) and 48 hours (squares) after IRI. Contralateral (Cntrl) kidneys are used as controls. [Neutrophils: *Dpep1*$^{+/+}$ (24 hours) Cntrl versus IRI, $^{**}P = 0.005$; IRI (24 hours) *Dpep1*$^{+/+}$ versus *Dpep1*$^{-/-}$, $^{**}P = 0.008$; *Dpep1*$^{+/+}$ (48 hours) Cntrl versus IRI, $^{**}P = 0.006$; IRI (48 hours) *Dpep1*$^{+/+}$ versus *Dpep1*$^{-/-}$, $^{***}P = 0.001$; $n = 5$ per group, Student's *t* test.] [Monocytes: *Dpep1*$^{+/+}$ (24 hours) Cntrl versus IRI, $^{***}P = 0.001$; IRI (24 hours) *Dpep1*$^{+/+}$ versus *Dpep1*$^{-/-}$, $^{**}P = 0.004$; *Dpep1*$^{+/+}$ (48 hours) Cntrl versus IRI, $^{**}P = 0.004$; IRI (48 hours) *Dpep1*$^{+/+}$ versus *Dpep1*$^{-/-}$, ns = not significant; $n = 5$ per group, Student's *t* test.] Flow cytometry of neutrophil (**C**) and inflammatory monocyte (**D**) recruitment to the kidneys of LSALT peptide–treated mice at 24 hours (circles) and 48 hours (squares) after IRI. Contralateral (Cntrl) kidneys are used as controls. [Neutrophils: Cntrl versus IRI (24 hours), $^{**}P = 0.005$; IRI (24 hours) no treatment versus LSALT, $^{**}P = 0.01$; Cntrl versus IRI (48 hours), $^{*}P = 0.048$; IRI (48 hours) no treatment versus LSALT, $^{*}P = 0.04$; $n = 6$ to 8 per group, Student's *t* test.] [Monocytes: Cntrl versus IRI (24 hours), $^{***}P = 0.0003$; IRI (24 hours) no treatment versus LSALT, $^{**}P = 0.005$; Cntrl versus IRI (48 hours), $^{**}P = 0.002$; IRI (48 hours) no treatment versus LSALT, $^{*}P = 0.047$; $n = 5$ to 8 per group, Student's *t* test.]

adhesion receptors in the tubulointerstitial compartment of the kidney during IRI (*16*, *18*, *19*). However, redundant pathways mediating renal inflammation are suggested because of the incomplete suppression of leukocyte recruitment observed when CD44 and ICAM-1 are individually targeted. To determine the relative importance of DPEP1 compared with CD44 and ICAM-1 in renal leukocyte recruitment, flow cytometry studies were conducted in *LysM*$^{gfp/gfp}$ mice undergoing IRI and treated with CD44 and/or ICAM-1–blocking antibodies. Leukocyte adhesion was first examined at early time points after IRI using IVM. Both CD44 and DPEP1 blockade, using the IM7 antibody (*30*) or LSALT peptide, respectively, prevented the adhesion of GFP^{+} leukocytes to the kidney at 2 hours after IRI (Fig. 6, A and B). In contrast, ICAM-1 blockade using the YN1/1.7.4 antibody (*31*) had little impact on renal inflammation at this time point. Studies were next performed analyzing total kidney GFP^{+} leukocyte subpopulations by flow cytometry (fig. S3). Whereas DPEP1 inhibition using the LSALT peptide reduced all GFP^{+} leukocyte populations to the kidney, including neutrophils and monocyte/macrophages, blocking ICAM-1 antibodies only inhibited GFP^{int} macrophages at 24 hours after IRI (Fig. 6, C and D). When administered with the LSALT peptide, ICAM-1 antibody was additive with a significant reduction observed in the recruitment of all GFP^{+} leukocytes (Fig. 6D). Blocking CD44 antibodies prevented the recruitment of both GFP^{int} macrophages and GFP^{hi} neutrophils and appeared to be slightly more effective than LSALT peptide in the recruitment of neutrophils (Fig. 6, C and D). Like ICAM-1, combining LSALT peptide with anti-CD44 antibodies provided an additive effect, reducing total leukocyte populations in the kidney further with an almost complete inhibition of neutrophil recruitment (Fig. 6D). Together, these results demonstrate that during experimental renal IRI, neutrophil recruitment is mediated primarily by CD44 and DPEP1, whereas the recruitment of inflammatory monocytes and macrophages involves all three molecules, including ICAM-1.

DPEP1-mediated leukocyte recruitment does not depend on tubular injury

DPEP1 plays a role in glutathione metabolism and has recently been implicated in ferroptosis, a key process in the pathogenesis of AKI (*7*, *25*, *32*). Thus, the reduction in leukocyte recruitment and inflammation observed following DPEP1 inhibition or deficiency during IRI may be an indirect result of DPEP1 effects on tubular injury and death. To investigate this possibility, expression of key ferroptosis

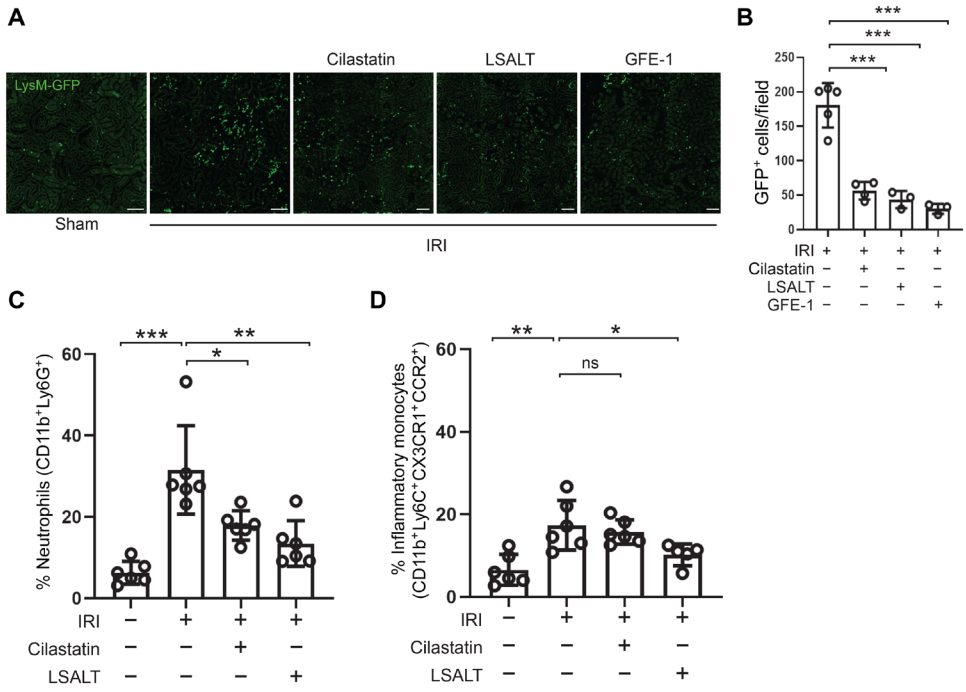

Fig. 4. DPEP1 inhibitors and leukocyte recruitment during kidney IRI. (**A**) Kidney IVM in *LysM*$^{gfp/gfp}$ mice at 2 hours following IRI in mice treated with LSALT peptide, cilastatin, or GFE-1 peptide. Sham-operated kidney is used as a negative control. Scale bars, 100 μm. (**B**) Stationary GFP$^+$ leukocytes/field in the kidney were quantified (versus IRI: cilastatin, ***$P = 0.0002$; LSALT, ***$P = 0.0005$; GFE-1, ***$P = 0.0003$; $n = 3$ to 5 per group, ANOVA with Dunnett's post hoc test). (**C** and **D**) Flow cytometry of leukocytes isolated from ischemic (IRI) and contralateral (Cntrl) kidneys in wild-type mice treated with or without cilastatin or LSALT peptide at 48 hours (neutrophils: Cntrl versus IRI, ***$P = 0.0006$; IRI versus IRI + cilastatin, *$P = 0.011$; IRI versus IRI + LSALT, $P = 0.001$; $n = 5$ to 6 per group, ANOVA with Dunnett's post hoc test) (inflammatory monocytes: Cntrl versus IRI, **$P = 0.01$; IRI versus IRI + cilastatin, ns = not significant; IRI versus IRI + LSAL, $P = 0.047$; $n = 5$ to 6 per group, ANOVA with Dunnett's post hoc test).

proteins and tissue glutathione levels in the kidney were assessed. At baseline, very little difference was observed in phospholipid hydroperoxide glutathione peroxidase (GPX4) and long-chain-fatty-acid-CoA ligase 4 (ACSL4) protein expression between *Dpep1*$^{+/+}$ and *Dpep1*$^{-/-}$ mice (Fig. 7A). The expression of LRP2 (low-density lipoprotein receptor-related protein 2 or megalin), a major luminal proximal tubular receptor that mediates selenoprotein P transport needed to maintain homeostasis of selenoproteins such as GPX4 (*33*), was also similar in *Dpep1*$^{-/-}$ compared with wild-type littermates at baseline (Fig. 7A and fig. S4A). At 48 hours following IRI, *Dpep1*$^{+/+}$ mice demonstrated a reduction in LRP2 and GPX4 protein expression compared with *Dpep1*$^{-/-}$ mice, whereas ACSL4 was induced similarly in both strains (Fig. 7A). Moreover, glutathione levels were generally increased in the kidneys of *Dpep1*$^{-/-}$ mice at baseline and following IRI (fig. S4, B and C). While these findings may be secondary to more severe tubular injury and loss in *Dpep1*$^{+/+}$ compared with *Dpep1*$^{-/-}$ mice, they are also consistent with enhanced ferroptosis in the wild-type mice. To further probe a direct role for DPEP1 in kidney leukocyte trafficking, IVM was used in *LysM*$^{gfp/gfp}$ mice immediately following the systemic administration of LPS, before any tubular cell injury could occur. Within 2 hours of LPS administration, a substantial influx of GFP$^+$ leukocytes could be detected within the kidney (Fig. 7B). The influx of leukocytes was significantly reduced in LPS-treated *Dpep1*$^{-/-}$ mice or mice pretreated with cilastatin or the LSALT peptide (Fig. 7, B to D). As expected, leukocyte recruitment in response to LPS occurred in the absence of overt tubular cell membrane disruption as measured by SYTOX Red staining (Fig. 7E). Together, these results show that DPEP1-mediated leukocyte recruitment to the kidney is direct and can occur in the absence of tubular injury or death. An additional contribution of DPEP1 to ferroptosis during AKI however remains possible.

DISCUSSION

In this paper, we identify a central role for DPEP1 in the pathogenesis of renal inflammation and the AKI phenotype induced by IRI. Furthermore, we clarify the biology of inflammation in the kidney and show that DPEP1 plays a major role in neutrophil and monocyte recruitment in conjunction with CD44 and ICAM-1. Last, our results identify therapeutic targeting of DPEP1 as a promising strategy to prevent AKI.

The biology of leukocyte recruitment in the kidney during IRI has not been fully elucidated. Previous studies have shown roles for the selectins in leukocyte rolling, and CD44 and ICAM-1 in leukocyte adhesion (*15*, *16*, *18*, *19*). However, residual leukocyte recruitment still occurred in mice lacking CD44 and/or ICAM-1, suggesting that redundant pathways exist in the kidney (*16*, *17*). Our data confirm DPEP1 as another major leukocyte adhesion receptor in the kidney that, in conjunction with CD44, regulates most of the neutrophil recruitment during experimental IRI. While ICAM-1 also contributes to leukocyte recruitment, its role appears to be more selective to the monocyte population, whereas CD44 and DPEP1 inhibit the recruitment of both neutrophils and monocytes during injury. These data are consistent with our group's recent work identifying DPEP1

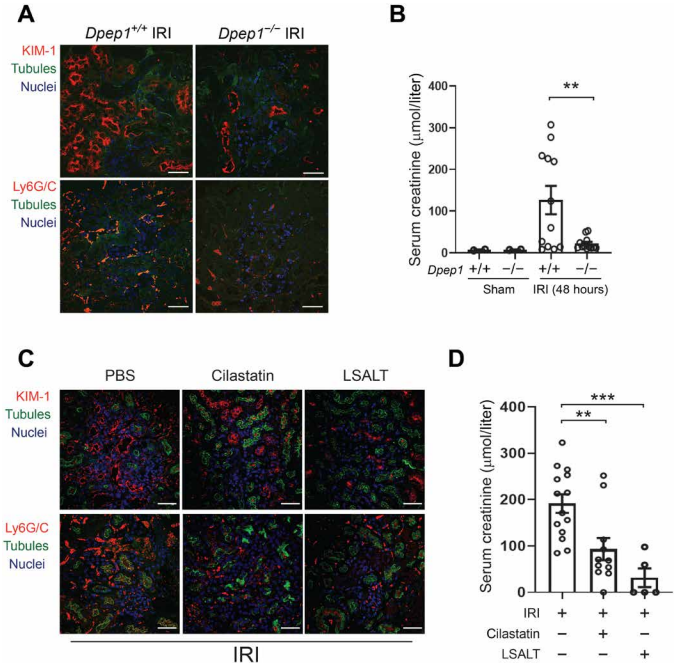

Fig. 5. Impact of DPEP1 on AKI phenotype during IRI. (**A**) Immunofluorescence confocal microscopy for KIM-1 and Ly6G/C in the kidneys of *Dpep1*$^{+/+}$ and *Dpep1*$^{-/-}$ mice 48 hours following renal IRI. Labels: KIM-1 (top, red), Ly6G/C (bottom, red), tubules (LTL, green), and nuclei [4′,6-diamidino-2-phenylindole (DAPI), blue]. Scale bars, 50 μm. (**B**) Renal function determined by serum creatinine in sham- and renal IRI–treated *Dpep1*$^{+/+}$ and *Dpep1*$^{-/-}$ mice at 48 hours (IRI *Dpep1*$^{+/+}$ versus *Dpep1*$^{-/-}$, $^{**}P = 0.007$; $n = 8$ per group, Student's t test). (**C**) Immunofluorescence confocal microscopy for KIM-1 and Ly6G/C in the kidneys of wild-type mice 48 hours following renal IRI with or without treatment with cilastatin or LSALT. Labels: KIM-1 (top, red), Ly6G/C (bottom, red), tubules (LTL, green), and nuclei (DAPI, blue). Scale bars, 50 μm. (**D**) Renal function determined by serum creatinine in renal IRI–treated mice with or without cilastatin or LSALT peptide at 48 hours (versus IRI alone: cilastatin, $^{**}P = 0.005$; LSALT, $^{***}P = 0.0005$; $n = 5$ to 14 per group, ANOVA with Dunnett's post hoc test).

as a leukocyte adhesion receptor in the lungs and liver (*14*) and the identification of DPEP1 expression in the peritubular capillaries shown in that study.

DPEP1 deficiency or inhibition substantially attenuated the phenotype of renal IRI in mice. The effects of DPEP1 in the pathogenesis of renal IRI may be multifactorial. First, inhibition of DPEP1 mediated inflammation, and leukocyte recruitment plays a major role in preventing severe manifestations of AKI. Second, preventing DPEP1 activation may affect tubular cell injury. Recent studies have suggested a role for DPEP1 in regulating ferroptosis [Linkermann, co-submission, and (*25*)], which is a major cause of cell death during AKI (*7*, *32*, *34*, *35*). In *Dpep1*$^{-/-}$ mice subjected to IRI, our data demonstrated an increase in tissue glutathione levels and GPX4 expression, molecules that are directly involved in the ferroptosis pathway. Last, DPEP1 inhibition may protect the kidney by preventing some of its tubular trafficking functions. Cilastatin has been shown to prevent toxin-induced AKI in part because of prevention of tubular uptake of drugs such as contrast agents (diatrizoate), cisplatin, and vancomycin (*26*, *27*, *36*). More recently, cilastatin was shown to prevent pigment-induced AKI caused by rhabdomyolysis, raising the possibility that DPEP1 also facilitates the uptake of endogenous damage-associated molecular patterns (DAMPs) (*37*) released in the tubular lumen during IRI. While the effects of cilastatin in these studies may be due to DPEP1's emerging role in ferroptosis, some studies suggest that cilastatin has off-target effects and prevents tubular molecular trafficking via LRP2 (*36*, *38*). However, LRP2 is a major luminal receptor in the proximal tubule, which may limit ferroptosis by promoting cellular selenoprotein synthesis through its handling of selenoprotein P (*33*). Further research is needed to fully understand the biology of DPEP1 and cilastatin in tubular molecular trafficking and its impact on kidney disease. Given that both enzymatic and nonenzymatic DPEP1 inhibition were effective in attenuating the IRI phenotype, it is likely that DPEP1 regulates multiple pathways that contribute to the pathogenesis of renal IRI and AKI in general.

The data here identify DPEP1 as a major leukocyte adhesion receptor in the kidney and a multifunctional protein in the pathogenesis of AKI. Furthermore, we identify two therapeutic agents that could be applied in human clinical trials. First is the LSALT peptide, which showed significant efficacy attenuating kidney inflammation during experimental IRI. Since inflammation plays a role in many different etiologies of AKI, targeting DPEP1-mediated inflammation represents a rational therapeutic approach in humans. Second is cilastatin, a drug that was first developed to prevent the metabolism of imipenem in the kidney (*24*). Cilastatin effects in the kidney may be more pleiotropic because of its mechanism of action, affecting tubular cell biology in addition to regulating DPEP1-mediated inflammation. Given its long track record of use in humans, cilastatin could easily be evaluated clinically. Targeting DPEP1 using cilastatin and/or LSALT peptide warrants further testing in human clinical trials for AKI.

MATERIALS AND METHODS

Mice

Wild-type and *LysM*$^{gfp/gfp}$ mice (*28*) were on a C57BL/6 background and housed under standard conditions. *Dpep1*$^{+/+}$ and *Dpep1*$^{-/-}$ littermates were used throughout the study and generated from *Dpep1*$^{+/-}$ breeders on a C57BL/6 background (*14*). Mice were used between 8 and 12 weeks of age. Both sexes of mice were used equally throughout the study. All studies were approved by the Animal Care Committee at the University of Calgary.

Experimental disease models

Renal IRI and AKI were induced by a surgical model of renal IRI in mice as previously described (*39*). Briefly, mice were anaesthetized using ketamine (100 mg/kg) and xylazine (10 mg/kg) supplemented with isofluorane. The left kidney was isolated through a small lateral incision, and a vascular clamp was applied to the renal pedicle. Ischemia was induced for 30 min at 34°C, followed by removal of the vascular clamp and recovery of the animals with supplemental heat, hydration, and pain relief. The unmanipulated right contralateral kidney was used as control. For renal function and pathology studies, a life-supporting renal IRI model was used, which involved a right nephrectomy before inducing ischemic injury to the left kidney. Sham-operated mice underwent nephrectomy and/or isolation of the left kidney only. Inhibitor studies in mice were performed using LSALT peptide [LSALTPSPSWLKYKAL, 17.75 μg/kg, intravenously (iv); CS Bio, USA] (*14*), GFE-1 peptide (CGFECVRQCPERC, 15.3 μg/kg, iv; Canpeptide, Canada) (*29*), cilastatin (17.9 mg/kg, iv; Tocris Bioscience, USA), anti–ICAM-1 antibody [200 μg, intraperitoneally (ip); clone YN1/1.7.4, BioXCell, USA] (*31*), or anti-CD44

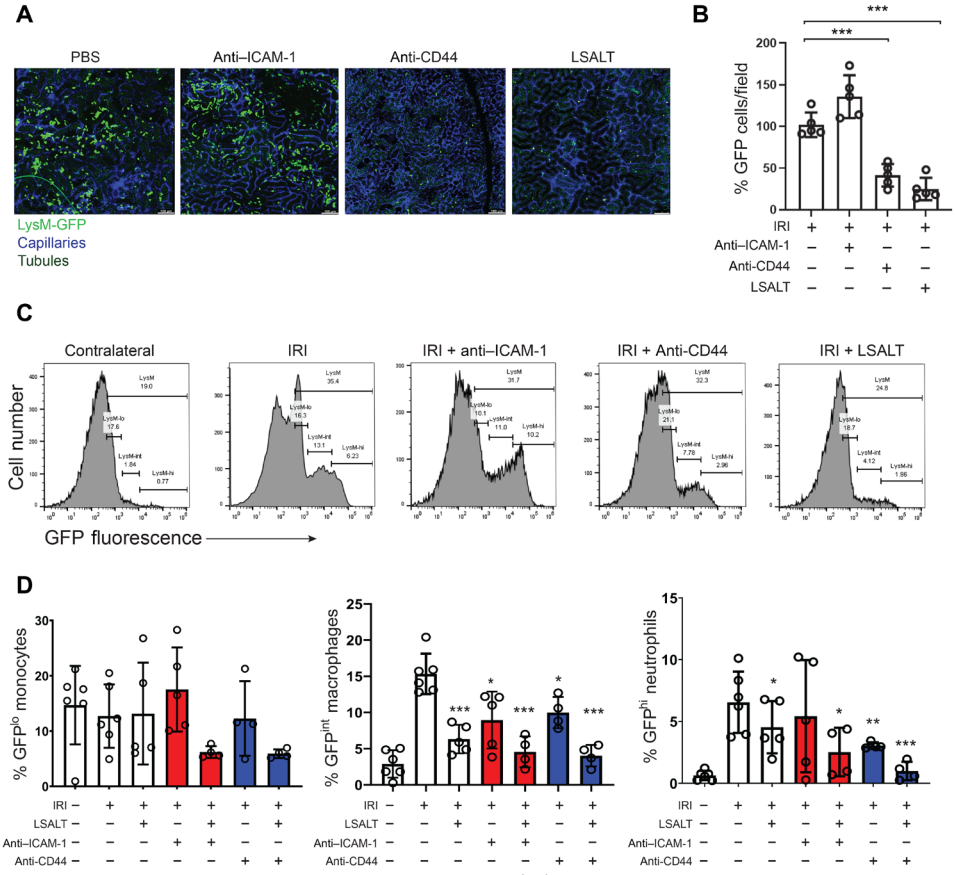

Fig. 6. Role of CD44 and ICAM-1 in IRI-induced renal inflammation. (**A**) IVM in *LysM*$^{gfp/gfp}$ mice at 2 hours following renal IRI with and without treatment with anti–ICAM-1, anti-CD44, or LSALT peptide. Labels: leukocytes (LysM-GFP, green), tubules (autofluorescence, dark green), and capillaries (QTracker, blue). Scale bars, 100 μm. (**B**) Stationary GFP$^+$ leukocytes/field in the kidney were quantified (IRI versus anti-CD44: ***$P = 0.0002$; LSALT: ***$P < 0.0001$, five per group, ANOVA with Tukey post hoc test). (**C**) Representative flow cytometry of kidney leukocytes isolated from *LysM*$^{gfp/gfp}$ mice 24 hours after IRI with or without LSALT peptide, CD44, or ICAM-1–blocking antibody treatment. Distinct GFP$^+$ leukocyte populations were characterized by flow cytometry (GFP^{lo} = monocytes, GFP^{int} = macrophages, and GFP^{hi} = neutrophils). Contralateral kidneys from untreated IRI mice are used as controls. (**D**) Quantification of kidney GFP$^+$ leukocytes in *LysM*$^{gfp/gfp}$ mice 24 hours after IRI with and without treatment with LSALT peptide, anti–ICAM-1, and anti-CD44 antibodies. (GFP^{int} macrophages IRI versus LSALT, ***$P = 0.0002$; anti–ICAM-1, *$P = 0.017$; anti–ICAM-1 + LSALT, ***$P = 0.0006$; anti-CD44, *$P = 0.015$; anti-CD44 + LSALT, ***$P < 0.0001$. GFP^{hi} neutrophils IRI versus LSALT, *$P = 0.037$; anti–ICAM-1, P = ns; anti–ICAM-1 + LSALT, *$P = 0.034$; anti-CD44, **$P = 0.001$; anti-CD44 + LSALT, ***$P < 0.0001$. Four to six per group, ANOVA with Dunnett's post hoc test.)

antibody (100 μg, iv; clone IM7; BioXCell, USA) (*30*) administered as a single dose 30 min before IRI (anti–ICAM-1 was administered once daily 48 hours before IRI). Scrambled LSALT peptide (LWLPLKSATPSYALSK) consisting of randomized LSALT peptide amino acids was used as a control for LSALT peptide. For studies extending beyond 4 hours, cilastatin and the LSALT peptide were administered again at 4 and 24 hours after IRI.

Endotoxemia was induced using LPS (5 mg/kg, iv; O111:B4; InvivoGen, USA) treatment via intravenous administration. Inhibitor studies in mice were performed using LSALT peptide (17.75 mg/kg, iv; CS Bio, USA) (*14*) or cilastatin (17.9 mg/kg, iv; Tocris Bioscience, USA) administered once 30 min pre-LPS.

Kidney multiphoton IVM

Renal IVM was performed as previously described (*27*). Briefly, mice were anesthetized and tail veins catheterized for drug and reagent administration. The kidney was exteriorized using a lateral incision and extended over the heated imaging platform. Imaging was done with an SP5 Leica multiphoton confocal microscope (Leica, Germany) and MaiTai Ti-Sapphire laser (Spectra Physics, USA) at 800- to 850-nM excitation using predefined laser power and detector gain settings. Time-lapse imaging was acquired at 0.5 s per frame. Z stacks were acquired at 20-μm optical sections and 2-μm steps. The following reagents were administered intravenously to visualize physiological and cellular compartments: QTracker655 (Thermo Fisher Scientific, USA), phycoerythrin (PE)–conjugated anti-F4/80 (clone BM8, BioLegend, USA), PE-conjugated anti-CD11b (clone M1/70, BioLegend, USA), Alexa Fluor 568–conjugated LSALT peptide (conjugated using Protein Labeling Kit, Invitrogen, USA), and SYTOX Red (Thermo Fisher Scientific, USA). Native LASX software (Leica, Germany) was used for acquisition and image processing. Adherent leukocytes (LysM-GFP or antibody labeled) were manually counted in each field on the basis of their fixed position over the course of 2 min. A minimum of three fields were acquired and analyzed per mouse for quantification.

Immunoblotting

Protein was isolated from mouse kidney tissue using radioimmunoprecipitation assay buffer (Sigma-Aldrich, USA). Protein samples were separated by SDS–polyacrylamide gel electrophoresis gels under

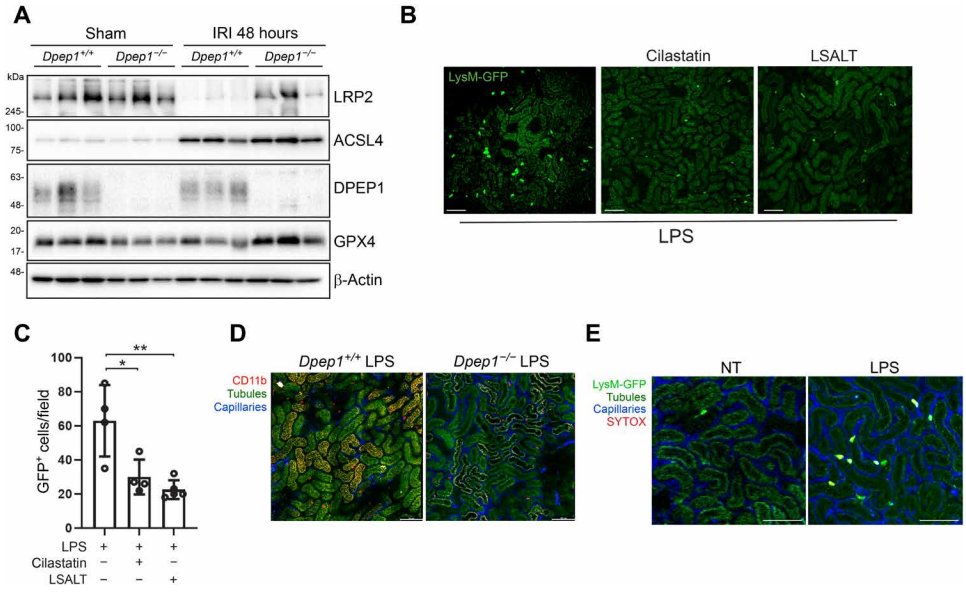

Fig. 7. DPEP1-mediated leukocyte recruitment and tubular injury. (**A**) Immunoblotting for LRP2, GPX4, ACSL4, and DPEP1 expression in whole-kidney tissue from *Dpep1*$^{-/-}$ and *Dpep1*$^{+/+}$ mice 48 hours after renal IRI or sham operation. (**B**) Kidney IVM in *LysM*$^{gfp/gfp}$ mice at 90 min following LPS administration with or without cilastatin or LSALT peptide treatment. Scale bars, 100 μm. (**C**) Stationary GFP^{+} leukocytes/field in the kidney were quantified (versus LPS: cilastatin, $^{*}P = 0.01$; LSALT, $^{**}P = 0.002$; $n = 4$ to 5 per group, ANOVA with Dunnett's post hoc test). (**D**) Kidney IVM in *Dpep1*$^{+/+}$ and *Dpep1*$^{-/-}$ mice at 90 min following LPS administration. Labels: leukocytes (CD11b, red), capillaries (QTracker, blue), and tubules (autofluorescence, yellow-green). Scale bars, 100 μm. (**E**) Kidney IVM with SYTOX Red staining in *LysM*$^{gfp/gfp}$ mice 2 hours following LPS administration. Non-LPS (NT)–treated mice are shown as a control. Labels: leukocytes (LysM-GFP, bright green/yellow), tubules (autofluorescence, dark green), capillaries (QTracker, blue), and necrotic cells (SYTOX, red). Scale bars, 100 μm.

reducing conditions. Proteins were transferred onto nitrocellulose membranes (GE Healthcare, USA) and blocked for 1 hour with blocking solution before overnight incubation at 4°C with primary antibody. Blots were washed and incubated with appropriate secondary antibody conjugated to horseradish peroxidase at room temperature. Proteins were visualized with enhanced chemiluminescence Western blotting detection reagents (Bio-Rad, USA) and digitally captured with a Chemidoc MP device (Bio-Rad, USA). Antibodies used are as follows: anti-DPEP1 (rabbit polyclonal, catalog no. MBS2521928, MyBioSource, USA), anti-GPX4 (clone EPNCIR144, catalog no. ab125066, Abcam, USA), anti-ACSL4 (rabbit polyclonal, catalog no. PA5-27137, Invitrogen, USA), anti-LRP2 (rabbit polyclonal, catalog no. 19700-I-AP, MyBiosource, USA), and anti–β-actin (clone hVIN-1, catalog no. V9131, Sigma-Aldrich, USA).

Flow cytometry

Kidney tissue was isolated from mice after perfusion via saline injection into the heart. Kidney capsule and fat were removed before mechanical and enzymatic digestion with the Multi Tissue Dissociation Kit I (Miltenyi Biotec, Germany) as per the manufacturer's instructions. Viable immune cells were isolated using a density gradient by mixing cells with Percoll (GE Healthcare, Sweden). For DPEP1 characterization, cells were labeled with the following antibodies: eFluor 450–conjugated anti-CD31 (clone 390, eBioscience, USA), fluorescein-conjugated LTL (catalog no. FL-1321, Vector Laboratories, USA), PE-conjugated anti-CD45 (clone 30-F11, BioLegend, USA), anti-DPEP1 (rabbit polyclonal, catalog no. MBS2521928, MyBioSource, USA), and Alexa 647–conjugated anti-rabbit immunoglobulin G (IgG) secondary antibody [clone (H + L), Invitrogen, USA]. For inflammatory response characterization, cells were labeled with the following antibodies: Brilliant Violet 421–conjugated anti-Ly6G (clone 1A8, BioLegend, USA), fluorescein isothiocyanate–conjugated anti-CD45 (clone 30-F11, BioLegend, USA), PE-conjugated anti-F4/80 (clone BM8, BioLegend, USA), PE/Cy7-conjugated anti-Ly6C (clone HK1.4, BioLegend, USA), APC-conjugated anti-CX_3CR1 (clone SA011F11, BioLegend, USA), APC/Cy7–conjugated CD11b (clone M1/70, BioLegend, USA), Alexa Fluor 700–conjugated CCR2 (clone 475301, R&D Systems, USA), PerCP-Cy5.5–conjugated anti-NK1.1 (clone PK136, Invitrogen, USA), PE-conjugated anti-CD3 (clone 145-2C11, Invitrogen, USA), PE/Cy7-conjugated CD4 (clone RM4-4, BioLegend, USA), APC/Cy7-conjugated anti-CD8 (clone 53-6.7, BD Pharmingen, USA), APC/Cy7-conjugated anti-CD11c (clone N418, BioLegend, USA), Pacific Blue–conjugated anti–I-A/I-E (major histocompatibility complex II) (clone M5/114.15.2, BioLegend, USA), and eFluor 450–conjugated anti-IgM (clone eB121-15F9, eBioscience, USA). Cells were analyzed using Attune NXT flow cytometer (Life Technologies, USA) and FlowJo software (BD Bioscience, USA).

Histological analysis of fixed renal tissue samples

For immunofluorescence, mouse kidneys were fixed in 10% neutral-buffered formalin and paraffinized before mounting onto slides. Tissue sections were deparaffinized, blocked, and labeled with the following antibodies: anti–KIM-1 (clone 222414, R&D Systems, USA), anti-Ly6G/C (clone NIMP-R14, Abcam, USA), and fluorescein-labeled LTL (Vector Laboratories, USA). Images were acquired using a confocal fluorescent microscope (Olympus IX-70) with Fluoview1000 software.

Immunohistochemistry was performed on formalin-fixed paraffin-embedded (FFPE) human kidney tissue samples obtained from the

Biobank for the Molecular Classification of Kidney Disease (University of Calgary). Control tissue was obtained from nondiseased margins of human nephrectomies that were performed for medical indications. All human studies were approved by the Conjoint Health Research Ethics Board at the University of Calgary and Alberta Health Services. FFPE human kidney tissues were deparaffinized, blocked, and labeled with the following antibodies: anti-DPEP1 (rabbit polyclonal, catalog no. 12222-1-AP, Proteintech, USA) and anti-rabbit isotype control (DAKO, USA). FFPE mouse kidney tissues were probed using anti-DPEP1 (rabbit polyclonal, catalog no. ab121308, Abcam, USA) and anti-LRP2 (clone H-10, catalog no. sc-515772, Santa Cruz Biotechnology, USA).

Glutathione assay

To measure mouse kidney tissue glutathione, runs were performed on a Q Exactive Hybrid Quadrupole-Orbitrap Mass Spectrometer (Thermo Fisher Scientific, USA) equipped with a heated electrospray ionization probe (HESI-II) and coupled to a Vanquish ultrahigh performance liquid chromatography (UHPLC) system (Thermo Fisher Scientific, USA). Chromatographic separation was achieved on a Syncronis HILIC UHPLC column (1.7 µm, 100 × 2.1 mm, Thermo Fisher Scientific, USA) using a binary solvent system at a flow rate of 600 µl/min with the following: solvent A, 20 mM ammonium formate (pH 3.0) in mass spectrometry grade H_2O; solvent B, mass spectrometry grade acetonitrile with 0.1% formic acid (%v/v). The gradient elution was as follows: 0 to 2 min, 100% B; 2 to 7 min, 80% B; 7 to 10 min, 5% B; 10 to 12 min, 5% B; 12 to 13 min, 100% B; and 13 to 15 min, 100% B. A sample injection volume of 2 µl was used. The column was kept at 30°C.

The mass spectrometer was run in negative full scan mode at a resolution of 140,000 scanning from 70 to 1000 m/z. The source settings were as follows: spray voltage, 2.5 kV; capillary temperature, 275°C; sheath gas, 25 (arbitrary unit); auxiliary gas, 10 (arbitrary unit); spare gas, 2 (arbitrary unit); and probe heater temperature, 325°C.

Glutathione in the samples was quantified using external standard calibration. A freshly prepared 50 mM glutathione stock solution was used to prepare 10 calibration solutions with concentrations ranging from 25 to 0.049 µM. Data analysis was conducted in El-MAVEN using integrated peak intensity (*40*).

Creatinine assays

Renal function was determined in mouse serum using a serum creatinine assay in the clinical laboratories of Alberta Precision Laboratories, a subsidiary of Alberta Health Services, Calgary, Alberta, Canada.

Statistical analysis

Data are shown as means ± SD. GraphPad Prism was used to perform all statistical analyses. Results were analyzed for statistical variance using unpaired two-tailed Student's t test or one-way analysis of variance (ANOVA) with Tukey or Dunnett's post hoc test where appropriate. Results at $P < 0.05$ were considered statistically significant. All experiments were performed at least three independent times.

SUPPLEMENTARY MATERIALS

Supplementary material for this article is available at https://science.org/doi/10.1126/sciadv.abm0142

View/request a protocol for this paper from *Bio-protocol*.

REFERENCES AND NOTES

1. M. T. James, W. A. Ghali, M. L. Knudtson, P. Ravani, M. Tonelli, P. Faris, N. Pannu, B. J. Manns, S. W. Klarenbach, B. R. Hemmelgarn; Alberta Provincial Project for Outcome Assessment in Coronary Heart Disease (APPROACH) Investigators, Associations between acute kidney injury and cardiovascular and renal outcomes after coronary angiography. *Circulation* **123**, 409–416 (2011).
2. M. T. James, A. S. Levey, M. Tonelli, Z. Tan, R. Barry, N. Pannu, P. Ravani, S. W. Klarenbach, B. J. Manns, B. R. Hemmelgarn, Incidence and prognosis of acute kidney diseases and disorders using an integrated approach to laboratory measurements in a universal health care system. *JAMA Netw. Open* **2**, e191795 (2019).
3. G. J. Nieuwenhuijs-Moeke, S. E. Pischke, S. P. Berger, J. S. F. Sanders, R. A. Pol, M. M. R. F. Struys, R. J. Ploeg, H. G. D. Leuvenink, Ischemia and reperfusion injury in kidney transplantation: Relevant mechanisms in injury and repair. *J. Clin. Med.* **9**, 253 (2020).
4. O. Rewa, S. M. Bagshaw, Acute kidney injury-epidemiology, outcomes and economics. *Nat. Rev. Nephrol.* **10**, 193–207 (2014).
5. Y. Wang, R. Bellomo, Cardiac surgery-associated acute kidney injury: Risk factors, pathophysiology and treatment. *Nat. Rev. Nephrol.* **13**, 697–711 (2017).
6. A. Linkermann, Nonapoptotic cell death in acute kidney injury and transplantation. *Kidney Int.* **89**, 46–57 (2016).
7. W. Tonnus, C. Meyer, C. Steinebach, A. Belavgeni, A. von Mässenhausen, N. Z. Gonzalez, F. Maremonti, F. Gembardt, N. Himmerkus, M. Latk, S. Locke, J. Marschner, W. Li, S. Short, S. Doll, I. Ingold, B. Proneth, C. Daniel, N. Kabgani, R. Kramann, S. Motika, P. J. Hergenrother, S. R. Bornstein, C. Hugo, J. U. Becker, K. Amann, H. J. Anders, D. Kreisel, D. Pratt, M. Gütschow, M. Conrad, A. Linkermann, Dysfunction of the key ferroptosis-surveilling systems hypersensitizes mice to tubular necrosis during acute kidney injury. *Nat. Commun.* **12**, 4402 (2021).
8. S. C. Huen, L. G. Cantley, Macrophages in renal injury and repair. *Annu. Rev. Physiol.* **79**, 449–469 (2017).
9. H. R. Jang, H. Rabb, Immune cells in experimental acute kidney injury. *Nat. Rev. Nephrol.* **11**, 88–101 (2015).
10. C. Stoppe, L. Averdunk, A. Goetzenich, J. Soppert, A. Marlier, S. Kraemer, J. Vieten, M. Coburn, A. Kowark, B.-S. Kim, G. Marx, S. Rex, A. Ochi, L. Leng, G. Moeckel, A. Linkermann, O. E. Bounkari, A. Zarbock, J. Bernhagen, S. Djudjaj, R. Bucala, P. Boor, The protective role of macrophage migration inhibitory factor in acute kidney injury after cardiac surgery. *Sci. Transl. Med.* **10**, eaan4886 (2018).
11. J. Puthumana, H. Thiessen-Philbrook, L. Xu, S. G. Coca, A. X. Garg, J. Himmelfarb, P. K. Bhatraju, T. A. Ikizler, E. D. Siew, L. B. Ware, K. D. Liu, A. S. Go, J. S. Kaufman, P. L. Kimmel, V. M. Chinchilli, L. G. Cantley, C. R. Parikh, Biomarkers of inflammation and repair in kidney disease progression. *J. Clin. Invest.* **131**, e139927 (2021).
12. E. Kolaczkowska, P. Kubes, Neutrophil recruitment and function in health and inflammation. *Nat. Rev. Immunol.* **13**, 159–175 (2013).
13. W. Y. Lee, P. Kubes, Leukocyte adhesion in the liver: Distinct adhesion paradigm from other organs. *J. Hepatol.* **48**, 504–512 (2008).
14. S. R. Choudhury, L. Babes, J. J. Rahn, B.-Y. Ahn, K.-A. R. Goring, J. C. King, A. Lau, B. Petri, X. Hao, A. K. Chojnacki, A. Thanabalasuriar, E. F. McAvoy, S. Tabariès, C. Schraeder, K. D. Patel, P. M. Siegel, K. A. Kopciuk, D. C. Schriemer, D. A. Muruve, M. M. Kelly, B. G. Yipp, P. Kubes, S. M. Robbins, Dipeptidase-1 is an adhesion receptor for neutrophil recruitment in lungs and liver. *Cell* **178**, 1205–1221.e17 (2019).
15. K. J. Kelly, W. W. Williams Jr., R. B. Colvin, J. V. Bonventre, Antibody to intercellular adhesion molecule 1 protects the kidney against ischemic injury. *Proc. Natl. Acad. Sci. U.S.A.* **91**, 812–816 (1994).
16. K. J. Kelly, W. W. Williams Jr., R. B. Colvin, S. M. Meehan, T. A. Springer, J. C. Gutierrez-Ramos, J. V. Bonventre, Intercellular adhesion molecule-1-deficient mice are protected against ischemic renal injury. *J. Clin. Invest.* **97**, 1056–1063 (1996).
17. K. M. Rouschop, M. E. Sewnath, N. Claessen, J. J. Roelofs, I. Hoedemaeker, R. van der Neut, J. Aten, S. T. Pals, J. J. Weening, S. Florquin, CD44 deficiency increases tubular damage but reduces renal fibrosis in obstructive nephropathy. *J. Am. Soc. Nephrol.* **15**, 674–686 (2004).
18. J. M. Herter, J. Rossaint, T. Spieker, A. Zarbock, Adhesion molecules involved in neutrophil recruitment during sepsis-induced acute kidney injury. *J. Innate Immun.* **6**, 597–606 (2014).
19. K. M. Rouschop, J. J. T. H. Roelofs, N. Claessen, P. da Costa Martins, J.-J. Zwaginga, S. T. Pals, J. J. Weening, S. Florquin, Protection against renal ischemia reperfusion injury by CD44 disruption. *J. Am. Soc. Nephrol.* **16**, 2034–2043 (2005).
20. Y. Nitanai, Y. Satow, H. Adachi, M. Tsujimoto, Crystal structure of human renal dipeptidase involved in beta-lactam hydrolysis. *J. Mol. Biol.* **321**, 177–184 (2002).
21. T. McIntyre, N. P. Curthoys, Renal catabolism of glutathione. Characterization of a particulate rat renal dipeptidase that catalyzes the hydrolysis of cysteinylglycine. *J. Biol. Chem.* **257**, 11915–11921 (1982).
22. B. J. Campbell, L. J. Forrester, W. L. Zahler, M. Burks, Beta-lactamase activity of purified and partially characterized human renal dipeptidase. *J. Biol. Chem.* **259**, 14586–14590 (1984).

23. M. Koller, J. Brom, M. Raulf, W. Konig, Cilastatin (MK 0791) is a potent and specific inhibitor of the renal leukotriene D4-dipeptidase. *Biochem. Biophys. Res. Commun.* **131**, 974–979 (1985).
24. S. R. Norrby, K. Alestig, B. Björnegård, L. Å. Burman, F. Ferber, J. L. Huber, K. H. Jones, F. M. Kahan, J. S. Kahan, H. Kropp, M. A. P. Meisinger, J. G. Sundelof, Urinary recovery of N-formimidoyl thienamycin (MK0787) as affected by coadministration of N-formimidoyl thienamycin dehydropeptidase inhibitors. *Antimicrob. Agents Chemother.* **23**, 300–307 (1983).
25. Y. Guan, X. Liang, Z. Ma, H. Hu, H. Liu, Z. Miao, A. Linkermann, J. N. Hellwege, B. F. Voight, K. Susztak, A single genetic locus controls both expression of DPEP1/CHMP1A and kidney disease development via ferroptosis. *Nat. Commun.* **12**, 5078 (2021).
26. S. Camano, A. Lazaro, E. Moreno-Gordaliza, A. M. Torres, C. de Lucas, B. Humanes, J. A. Lazaro, M. Milagros Gomez-Gomez, L. Bosca, A. Tejedor, Cilastatin attenuates cisplatin-induced proximal tubular cell damage. *J. Pharmacol. Exp. Ther.* **334**, 419–429 (2010).
27. A. Lau, H. Chung, T. Komada, J. M. Platnich, C. F. Sandall, S. R. Choudhury, J. Chun, V. Naumenko, B. G. J. Surewaard, M. C. Nelson, A. Ulke-Lemée, P. L. Beck, H. Benediktsson, A. M. Jevnikar, S. L. Snelgrove, M. J. Hickey, D. L. Senger, M. T. James, J. A. Macdonald, P. Kubes, C. N. Jenne, D. A. Muruve, Renal immune surveillance and dipeptidase-1 contribute to contrast-induced acute kidney injury. *J. Clin. Invest.* **128**, 2894–2913 (2018).
28. N. Faust, F. Varas, L. M. Kelly, S. Heck, T. Graf, Insertion of enhanced green fluorescent protein into the lysozyme gene creates mice with green fluorescent granulocytes and macrophages. *Blood* **96**, 719–726 (2000).
29. D. Rajotte, E. Ruoslahti, Membrane dipeptidase is the receptor for a lung-targeting peptide identified by in vivo phage display. *J. Biol. Chem.* **274**, 11593–11598 (1999).
30. J. Lesley, R. Schulte, R. Hyman, Binding of hyaluronic acid to lymphoid cell lines is inhibited by monoclonal antibodies against Pgp-1. *Exp. Cell Res.* **187**, 224–233 (1990).
31. K. J. Horley, C. Carpenito, B. Baker, F. Takei, Molecular cloning of murine intercellular adhesion molecule (ICAM-1). *EMBO J.* **8**, 2889–2896 (1989).
32. J. P. Friedmann Angeli, M. Schneider, B. Proneth, Y. Y. Tyurina, V. A. Tyurin, V. J. Hammond, N. Herbach, M. Aichler, A. Walch, E. Eggenhofer, D. Basavarajappa, O. Rådmark, S. Kobayashi, T. Seibt, H. Beck, F. Neff, I. Esposito, R. Wanke, H. Förster, O. Yefremova, M. Heinrichmeyer, G. W. Bornkamm, E. K. Geissler, S. B. Thomas, B. R. Stockwell, V. B. O'Donnell, V. E. Kagan, J. A. Schick, M. Conrad, Inactivation of the ferroptosis regulator Gpx4 triggers acute renal failure in mice. *Nat. Cell Biol.* **16**, 1180–1191 (2014).
33. J. Chiu-Ugalde, F. Theilig, T. Behrends, J. Drebes, C. Sieland, P. Subbarayal, J. Köhrle, A. Hammes, L. Schomburg, U. Schweizer, Mutation of megalin leads to urinary loss of selenoprotein P and selenium deficiency in serum, liver, kidneys and brain. *Biochem. J.* **431**, 103–111 (2010).
34. A. Linkermann, J. H. Brasen, M. Darding, M. K. Jin, A. B. Sanz, J. O. Heller, F. de Zen, R. Weinlich, A. Ortiz, H. Walczak, J. M. Weinberg, D. R. Green, U. Kunzendorf, S. Krautwald, Two independent pathways of regulated necrosis mediate ischemia-reperfusion injury. *Proc. Natl. Acad. Sci. U.S.A.* **110**, 12024–12029 (2013).
35. A. Belavgeni, C. Meyer, J. Stumpf, C. Hugo, A. Linkermann, Ferroptosis and necroptosis in the kidney. *Cell Chem. Biol.* **27**, 448–462 (2020).
36. B. Humanes, J. C. Jado, S. Camaño, V. López-Parra, A. M. Torres, L. A. Álvarez-Sala, E. Cercenado, A. Tejedor, A. Lázaro, Protective effects of cilastatin against vancomycin-induced nephrotoxicity. *Biomed. Res. Int.* **2015**, 1–12 (2015).
37. K. Matsushita, K. Mori, T. Saritas, M. B. Eiwaz, Y. Funahashi, M. N. Nickerson, J. F. Hebert, A. C. Munhall, J. A. McCormick, M. Yanagita, M. P. Hutchens, Cilastatin ameliorates rhabdomyolysis-induced AKI in mice. *J. Am. Soc. Nephrol.* **32**, 2579–2594 (2021).
38. Y. Hori, N. Aoki, S. Kuwahara, M. Hosojima, R. Kaseda, S. Goto, T. Iida, S. De, H. Kabasawa, R. Kaneko, H. Aoki, Y. Tanabe, H. Kagamu, I. Narita, T. Kikuchi, A. Saito, Megalin blockade with cilastatin suppresses drug-induced nephrotoxicity. *J. Am. Soc. Nephrol.* **28**, 1783–1791 (2017).
39. A. Lau, S. Wang, J. Jiang, A. Haig, A. Pavlosky, A. Linkermann, Z. X. Zhang, A. M. Jevnikar, RIPK3-mediated necroptosis promotes donor kidney inflammatory injury and reduces allograft survival. *Am. J. Transplant.* **13**, 2805–2818 (2013).
40. S. Agrawal, S. Kumar, R. Sehgal, S. George, R. Gupta, S. Poddar, A. Jha, S. Pathak, El-MAVEN: A fast, robust, and user-friendly mass spectrometry data processing engine for metabolomics. *Methods Mol. Biol.* **1978**, 301–321 (2019).

Acknowledgments: Metabolomics data were obtained at the Calgary Metabolomics Research Facility (CMRF), which is supported by the International Microbiome Center at the University of Calgary. Infrastructure and technical support was also provided by K. Chapman, the Flow Cytometry Facility, Live Cell Imaging Facility, and the Biobank for the Molecular Classification of Kidney Disease at the Snyder Institute for Chronic Diseases, University of Calgary. **Funding:** This work was supported by operating grants from the Canadian Institutes for Health Research, the Kidney Foundation of Canada, and infrastructure grants from the Canada Foundation for Innovation. A.La. and J.J.R. receive salary support in part from a grant provided by Arch Biopartners Inc. I.A.L. is supported by an Alberta Innovates Translational Health Chair.
Author contributions: A.La. performed the majority of the experiments, data analysis, and wrote the manuscript. J.J.R., M.C., and H.C. conducted experiments and collected and analyzed the data. H.B. reviewed human renal pathology. C.N.J. contributed to the infrastructure and experimental design for IVM. D.B. and I.A.L. conducted metabolomics and glutathione assay. A.v.M. and A.Li. contributed to the conceptual and experimental design. S.M.R. and D.L.S. contributed reagents and to the conceptual and experimental design. J.C. contributed to the conceptual experimental design, supervised trainees, and contributed to data analysis. All authors reviewed the manuscript. D.A.M. oversaw the entire project, analyzed the data, and wrote the manuscript. **Competing interests:** D.A.M. is a cofounder and holds an equity position in Arch Biopartners Inc. A.La. and J.R. hold equity positions in Arch Biopartners Inc. S.M.R. and D.L.S. are cofounders of Arch Cancer Therapeutics Inc. and hold equity positions in Arch Biopartners Inc. A.La., D.A.M., J.J.R., S.M.R., and D.L.S. are co-inventors on the following patents filed by Arch Biopartners Inc.: (i) U.S. patent application #14/622177, filed 13 February 2015, publication 13 August 2015; international application #PCT/CA2015/000078, filed 13 February 2015, publication 20 August 2015; (ii) U.S. patent application #15/234521, filed 11 August 2016, publication 14 September 2017; international application #PCT/IB2016/001244, filed 11 August 2016, publication 16 February 2017; and (iii) U.S. patent application #16/700901, filed 2 December 2019, publication 16 July 2020; international application #PCT/IB2019/001289, filed 2 December 2019, publication 4 June 2020. The authors declare that they have no other competing interests. **Data and materials availability:** All data needed to evaluate the conclusions in the paper are present in the paper and/or the Supplementary Materials.

Submitted 20 August 2021
Accepted 8 December 2021
Published 2 February 2022
10.1126/sciadv.abm0142